PAPER

Effect of Nb and Cu on the crystallization behavior of under-stoichiometric Nd–Fe–B alloys

IOP Publishing Journal of Physics D: Applied Physics

J. Phys. D: Appl. Phys. **50** (2017) 015305 (8pp) doi:10.1088/1361-6463/50/1/015305

Effect of Nb and Cu on the crystallization behavior of under-stoichiometric Nd–Fe–B alloys

D Salazar[1], A Martín-Cid[1], R Madugundo[1,2], J S Garitaonandia[3], J M Barandiaran[1,3] and G C Hadjipanayis[2]

[1] BCMaterials, Bizkaia Science and Technology Park, E-48160 Derio, Spain
[2] Department of Physics and Astronomy, University of Delaware, Newark, DE 19716, USA
[3] Faculty of Science and Technology, University of the Basque Country (UPV/EHU) E-48080 Bilbao, Spain

E-mail: daniel.salazar@bcmaterials.net

Received 6 June 2016, revised 30 September 2016
Accepted for publication 19 October 2016
Published 23 November 2016

Abstract

In this work, we present a complete study of the influence of Nb and Cu addition on the crystallization behavior of Nd-lean Nd–Fe–B melt-spun alloys. Alloys with compositions $Nd_{10-x-y}Fe_{84}B_6Nb_xCu_y$ ($x = 1$, $y = 0$ and $x = 0.5$, $y = 0.5$) were melt-spun at different wheel speeds (15–40 m s^{-1}) to obtain samples in amorphous, highly disordered and nanocrystalline structures. The crystallization process, induced by different heat treatments, was studied by means of differential thermal analysis and x-ray powder thermodiffraction. Magnetic properties of as-made and heat-treated ribbons were measured by magnetometry. The as-made amorphous samples showed a crystallization to the 2:14:1 hard magnetic phase at $T_1 \sim 350$ °C. Doping with Nb results in an increase of T_1, and addition of Cu lowers T_1. This behavior is explained in terms of an inhibition of grain growth by Nb and a nucleation enhancement by Cu additions. During the crystallization process, a secondary phase (identified as a bcc-Fe-rich phase) is formed. The amount of such a phase increases with the annealing temperature. Coercivity increases upon annealing reaching maxima at 700–750 °C. This can be explained in terms of competition between the two phases formed: the 2:14:1 hard phase and the soft bcc-Fe-rich phase. The highest coercivity of the Nd-lean samples is observed when the microstructure is appropriate and both phases are exchange-coupled.

Keywords: amorphous ribbons, nanocrystallization, rare-earth-lean permanent magnet

S Online supplementary data available from stacks.iop.org/JPhysD/50/015305/mmedia

(Some figures may appear in colour only in the online journal)

1. Introduction

Nd–Fe–B magnets can be found in almost every modern-day electrical device. Certain applications demand that these magnets operate at high temperatures (above 150 °C), such as electrical vehicle motors and wind-turbine generators. These applications require high coercivity, which can be obtained in Dy/Tb-substituted Nd–Fe–B magnets. However, both Dy and Tb are critical and strategic raw materials [1], and the recent rare-earth crisis calls for rare-earth-lean or rare-earth-free permanent magnets. Melt-spun Nd-lean Nd–Fe–B alloys are potential candidates for the development of nanocomposite magnets consisting of magnetically hard $Nd_2Fe_{14}B$ grains exchange-coupled with magnetically soft α-Fe grains [2]. Usually, the coercivity of these magnets is rather low, but could be enhanced substantially with grain-boundary infiltration [2]. Therefore, it is very important to gain a better understanding of the crystallization processes and the final

microstructure in melt-spun Nd–Fe–B alloys before infiltration [2, 3]. In this sense, many researchers have been working to identify the best fabrication conditions to obtain exchange-coupled nanocomposite Nd–Fe–B-based permanent magnets [4–6]. Much of the research has been focused on amorphous samples where different fabrication methods (melt-spinning, mechanical alloying) and annealing treatments were investigated to obtain the best properties. The type and amount of different amorphous/disordered phases obtained by melt-spinning can be controlled using different wheel speeds [7] and can be well tuned by small substitutions of Nb [8, 9] avoiding any secondary heat treatment. However, this results in a high structural inhomogeneity when compared with the heat-treated samples. In order to make the microstructure of rare-earth-lean Nd–Fe–B magnets uniform, non-conventional annealing processes have been used. Flash annealing, which allows temperatures up to 750 °C to be reached in 30 s, was used to anneal Nd(Pr)-lean samples leading to exchange-coupled magnets with a grain size of 20 nm [10]. High-pressure-torsion deformation was used to induce plastic deformations in as-spun ribbons of Nd-lean Nd–Fe–B magnets [11], where the authors reported the formation of a nanocrystalline α-Fe phase embedded in amorphous Nd–Fe–B with a homogeneous distribution. Other works were focused on the influence of doping on the crystallization behavior [12, 13]; for example, the addition of Co and Zr in fast-annealed Nd-lean Nd–Fe–B samples resulted in an improvement of coercivity and remanence [12]. Additionally, the Curie temperature was found to increase with Co and decrease with Zr additions. Other authors reported the effect of Nb, Co, Cu and Ga in as-spun Nd–Fe–B ribbons where fast annealing under an external magnetic field of 0.8 T showed an increase in coercivity in samples with Co [13].

In the special case of samples doped with Nb and Cu, Zhang *et al* studied the effect of Nb in Nd–Dy–Fe–B permanent magnets and found that small Nb substitution makes the grains smaller and more homogeneous [14] enhancing the exchange coupling, which leads to a significant increase of coercivity with a slight decrease of remanence. Other compositions of Nd-lean-based (Nd–Fe–Co–B) were studied with Nb and Cu substitution by Wu *et al* [15] who found that the amorphous phase at the grain boundaries is enriched with Nb and B, making this phase more stable. This amorphous phase controls the grain growth during the fabrication process. Nb plays an important role during annealing, controlling the sample microstructure while Cu does not show a substantial influence on microstructure or on magnetic properties of these alloys because their significant amount of Co may enlarge the solubility of Cu, inhibiting the clustering of Cu atoms. In this work, we present our recent results on the crystallization processes in Dy-free Nd-lean Nd–Fe–B samples with small additions of Nb and Cu. X-ray thermodiffraction and calorimetry DSC (differential scanning calorimetry) measurements were performed on as-spun amorphous ribbons to detect the crystallization/formation temperature of different phases formed with the treatment. After determining the crystallization temperatures, we performed several heat treatments at different times and at temperatures close to those determined by the thermal analysis data, and monitored the development of coercivity with annealing. In order to understand the influence of Nb and Cu on the crystallization and resulting properties, samples which showed the maximum coercive field were used to study their structure by x-ray diffraction (XRD) and Mössbauer spectroscopy, and to determine and quantify the different phases formed during crystallization. A strong relationship was found between the amount of the phases present, their grain size, the magnetic properties that depend on their microstructure and the exchange coupling between the two phases.

2. Experimental

Alloys with compositions $Nd_{12}Fe_{81}B_6Nb_1$, $Nd_{10}Fe_{84}B_6$, $Nd_9Fe_{84}B_6Nb_1$ and $Nd_9Fe_{84}B_6Nb_{0.5}Cu_{0.5}$ were prepared by arc-melting the pure constituents under Ar atmosphere (table 1). Pieces of as-cast samples were melt-spun using an induction furnace on a Cu wheel at wheel speeds of 15–40 m s^{-1} under Ar gas. In order to induce the crystallization of the amorphous ribbons, the samples were annealed at high temperatures after sealing them in quartz tubes under vacuum to avoid oxidation during the heat treatment. No reaction of our samples with the quartz tubes was evidenced at any of the temperatures used. Heat treatments were performed between 600 and 800 °C and for times from 15 to 120 min. Hysteresis loops were obtained at room temperature using a vibrating sample magnetometer EZ7-VSM from Microsense, with the magnetic field applied along the ribbon length so that the self-demagnetization effect was negligible. Simultaneously, the crystallization of amorphous ribbons was investigated by means of differential thermal analysis (DTA, Setaram 92-16.18) and x-ray thermodiffraction measurements using temperature ramps of 20 and 5 K min^{-1}, respectively, to determine the different thermal processes and phases formed in the samples during the heat treatment. The XRD measurements on heat-treated samples were made on a Philips X'Pert Pro diffractometer, in the Bragg-Brentano geometry, with Cu K_α radiation ($\lambda = 1.5418$ Å). The samples were placed on a spinner to avoid a possible preferential crystalline orientation. The diffractograms were refined by Rietveld method, using the FullProf suite, in order to obtain the amount of phases present in the samples and their grain size estimated by means of the Williamson–Hall method. ^{57}Fe Mossbauer spectra were acquired at room temperature using a constant acceleration, transmission spectrometer with a ^{57}Co-Rh source. Calibration of the spectrometer and isomer shifts were referred to bcc-Fe at 295 K. This technique has often been used to gain information about iron-containing phases and the relative percentages of these phases formed during the crystallization process. Direct measurements of the microstructure on heat-treated samples were studied by means of scanning electron microscopy (SEM, JEOL JSM-6400).

Table 1. Sample compositions, sample notation and crystallization temperature of the Nd–Fe–B phase (T_1) and the α-Fe (T_2) determined by DTA and XRD.

Sample	Quote	$T_{1\text{-DTA}}$ (°C)	$T_{1\text{-XRD}}$ (°C)	$T_{2\text{-DTA}}$ (°C)	$T_{2\text{-XRD}}$ (°C)
$Nd_{10}Fe_{84}B_6$ at 26 m s^{-1}	10NFB_26	323–367	360	577	600
$Nd_9Fe_{84}B_6Nb_{0.5}Cu_{0.5}$ at 40 m s^{-1}	9NFBNC_40	265–342	415	595	—
$Nd_9Fe_{84}B_6Nb_1$ at 40 m s^{-1}	9NFBN_40	351–376	440	610	—
$Nd_9Fe_{84}B_6Nb_{0.5}Cu_{0.5}$ at 15 m s^{-1}	9NFBNC_15	—	—	—	—
$Nd_{12}Fe_{81}B_6Nb_1$ at 26 m s^{-1}	12NFBN_26	276–348	—	611	—

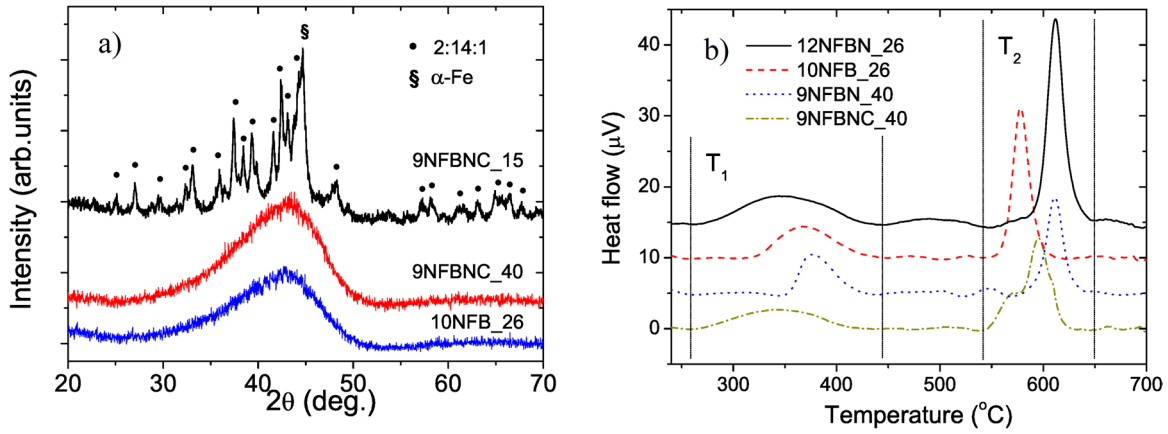

Figure 1. (a) XRD of selected as-spun samples and (b) DTA analysis of crystallization processes in amorphous Nd–Fe–B-based samples.

3. Results and discussion

3.1. Crystallization temperatures

The XRD spectra for ribbons spun at different wheel speeds and the DTA measurements for all the alloys are shown in figure 1. The x-ray spectra show the amorphous state of samples spun at 26 and 40 m s^{-1}, while for the sample spun at 15 m s^{-1} a crystalline ordering is observed (figure 1(a)). Crystalline phases of 9NFBNC_15 as-spun ribbons correspond to the 2:14:1 hard magnetic phase (•) and the secondary α-Fe phase (§), formed by the Fe excess in the alloy. The DTA data (figure 1(b)) show two exothermic peaks: the first, broader, peak at temperatures around T_1 (~350 °C) corresponds to the crystallization of the $Nd_2Fe_{14}B$ phase (as shown in figure 2), while the second one, a better defined peak at a higher temperature (T_2 ~ 600 °C), can be associated to the crystallization of a bcc-Fe-rich phase: the α-Fe phase. Table 1 shows the influence of the Nb and Cu addition on the crystallization of the samples. Addition of Nb increases T_2 from 577 °C in samples without Nb to 611 °C in samples with 1 at% Nb (9NFBN_40). Furthermore, the intensity of the T_2 peak is higher in samples made with lower wheel speed (26 m s^{-1}) and this may also be associated with the presence of an α-Fe nuclei, which already exists in the as-spun sample and they act as facilitators for the crystal growth. This is also consistent with the observation that more amorphous samples show a lower intensity T_2 peak. The onset of the first peak is associated with the nucleation, and the influence of the addition of Cu is clearly observed as a decrease on the nucleation temperature. Therefore, the onset of crystallization occurs earlier in the sample with Cu (9NFBNC_40), T_1 ~ 265 °C, than in the one without Cu (9NFBN_40), T_1 ~ 351 °C. These results suggest that the crystallization temperatures, for both the main and secondary phase, depend mainly on the addition of Nb and Cu, while the initial structural state of the sample has less influence.

The thermal processes described previously are related with the nucleation of stable phases and can be associated with the formation of their corresponding crystalline structures, which can be quantitatively identified by XRD experiments on annealed amorphous samples at the crystallization temperatures.

3.2. X-ray diffraction of crystallized samples

The crystal structures, and the amount of each crystallized phase, can be obtained by XRD experiments on samples annealed at the crystallization temperatures T_1 and T_2.

X-ray thermodiffraction spectra for (a) 10NFB_26, (b) 9NFBNC_40 and (c) 9NFBN_40 are shown in figure 2. To avoid the contribution of the Pt sample-holder used during experiments, caused by its diffraction peaks at 2θ–39° and 45° overlapping with the characteristic peak of α-Fe phase around 45° (see figure 1(a)), x-ray spectra are presented between 30°–37° and 47°–54°. Therefore, it was not possible to observe the formation of the α-Fe phase clearly, except for the 10NFB_26 sample where the slight appearance of an additional peak slightly below 45° is observed in the inset of figure 2. The α-Fe crystallization temperature in this sample is around 600 °C, close to the value obtained by the DTA method. On the other hand, the formation of $Nd_2Fe_{14}B$ hard magnetic phase is clearly observed in all spectra at temperatures around 350 °C. The most intense peaks are the first to appear, indicating the start of the crystallization. A comparison with the DTA data

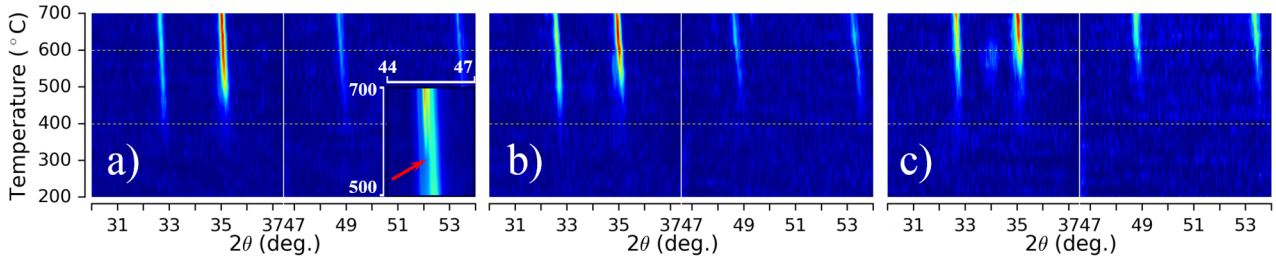

Figure 2. Thermodiffraction profiles of amorphous ribbons: (a) 10NFB_26, (b) 9NFBNC_40 and (c) 9NFBN_40. Inset: evidence of splitting of diffraction peak corresponding to Pt at $2\theta = 45°$ due to the crystallization of α-Fe phase.

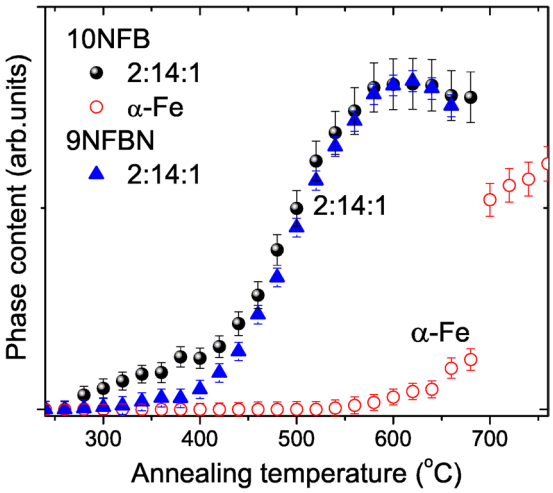

Figure 3. Formation of phases obtained from x-ray thermodiffraction profiles fitted by the Rietveld method.

seems to indicate that crystallization occurs at higher temperatures in the XRD experiment. We should note that the XRD peaks appear when there is a minimum of crystalline order in the sample, which occurs at temperatures higher than the onset of the crystallization process detected by calorimetry.

Through a Rietveld analysis of the x-ray thermodiffractions one can obtain the amount of different phases that appear during annealing and the temperature at which they are formed. The results of these refinements are shown in figure 3. Analytically, the formation and evolution of $Nd_2Fe_{14}B$ and α-Fe phases during heat treatments can be monitored.

3.3. Optimization of coercivity

With these results in mind, the optimum heat treatments for the crystallization of amorphous ribbons must be done at temperatures between those of both crystallization processes with the intention of obtaining $Nd_2Fe_{14}B$ grains with the optimum size and without an excessive amount of α-Fe phase in order to obtain the maximum coercivity [16]. The coercivity of powdered magnets increases with the reduction of particle size going through a maximum at the single domain size [16]. A series of heat treatments was performed on amorphous ribbons at temperatures between 600 and 800 °C and at times from 15 to 120 min to obtain samples with different grain sizes and α-Fe content to optimize their hard magnetic properties. Representative results are shown in figure 4. The inset shows the maximum coercivity obtained for each annealing temperature.

The amorphous/highly disordered ribbons show a very small coercivity. The coercivity of the ribbons increases abruptly with the annealing temperature up to a critical temperature; beyond this temperature the amount/size of α-Fe phase (soft magnetic phase) is large, promoting easy nucleation of reversed domains, which leads to lower coercivity. In the early stages of heat treatment, a nanocomposite structure is formed which consists of a mixture of $Nd_2Fe_{14}B$ hard magnetic phase and α-Fe soft phase. According to the exchange-spring magnet model [17], these two phases are exchange-coupled when the size of soft phase is around 10 nm (for Nd–Fe–B), resulting in an increase of remanence and a slight decrease of coercivity. The magnetic hysteresis loops in figure 4 do reflect the different microstructure of the treated samples. For instance, the samples heat-treated at 650 °C show a constricted shape hysteresis loop indicating the presence of two uncoupled phases. For most amorphous samples, 9NFBN_40 and 9NFBNC_40, the maximum H_c was obtained after annealing at 750 °C for 120 and 60 min showing a reduced remanence $m_R = M_R/M_s$ of 0.64 and 0.57 (M_s value was obtained by the law of approach to saturation), respectively, ensuring a good exchange coupling between the two magnetic phases. Samples heat-treated at higher temperatures or longer times showed a decreased coercivity caused by the higher amount and larger size of α-Fe which inhibits exchange coupling, again resulting in constricted loops with lower H_c.

The results of all heat treatments are summarized in figure 5. Since the addition of Nb in these alloys helps to inhibit grain growth [15], annealing was done at higher temperatures (~650 °C) in the Nb-containing samples. However, we found some discrepancies with the results obtained by Wu's group [15] in samples with Cu addition. In our case, Cu facilitates the nucleation of the hard magnetic phase and, therefore, it can promote grain growth at lower temperatures. This effect can be observed in our samples because the influence of Co on the crystallization is not present in our compounds (our samples do not contain Co). Consequently, one can obtain samples with different microstructures at the same annealing conditions by the addition of Nb and Cu.

The highest H_c was obtained in near-stoichiometric alloys 12NFBN_26 (H_c ~ 11 kOe), which were heat-treated between 650 and 700 °C. For under-stoichiometric Nd-lean Nd–Fe–B–Nb–Cu ribbons produced at 40 m s^{-1}, the maximum coercivity is obtained at 750 °C after 60 min annealing (H_c ~ 3.7 kOe)

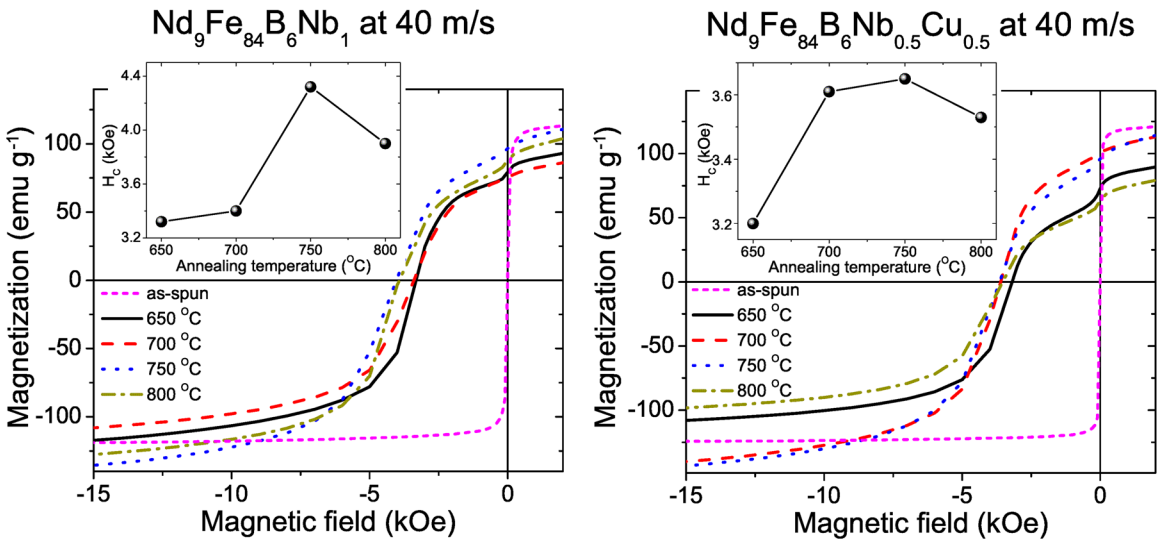

Figure 4. Hysteresis loops of samples (a) 9NFBN_40 and (b) 9NFBNC_40 heat-treated between 650 and 800 °C at different times.

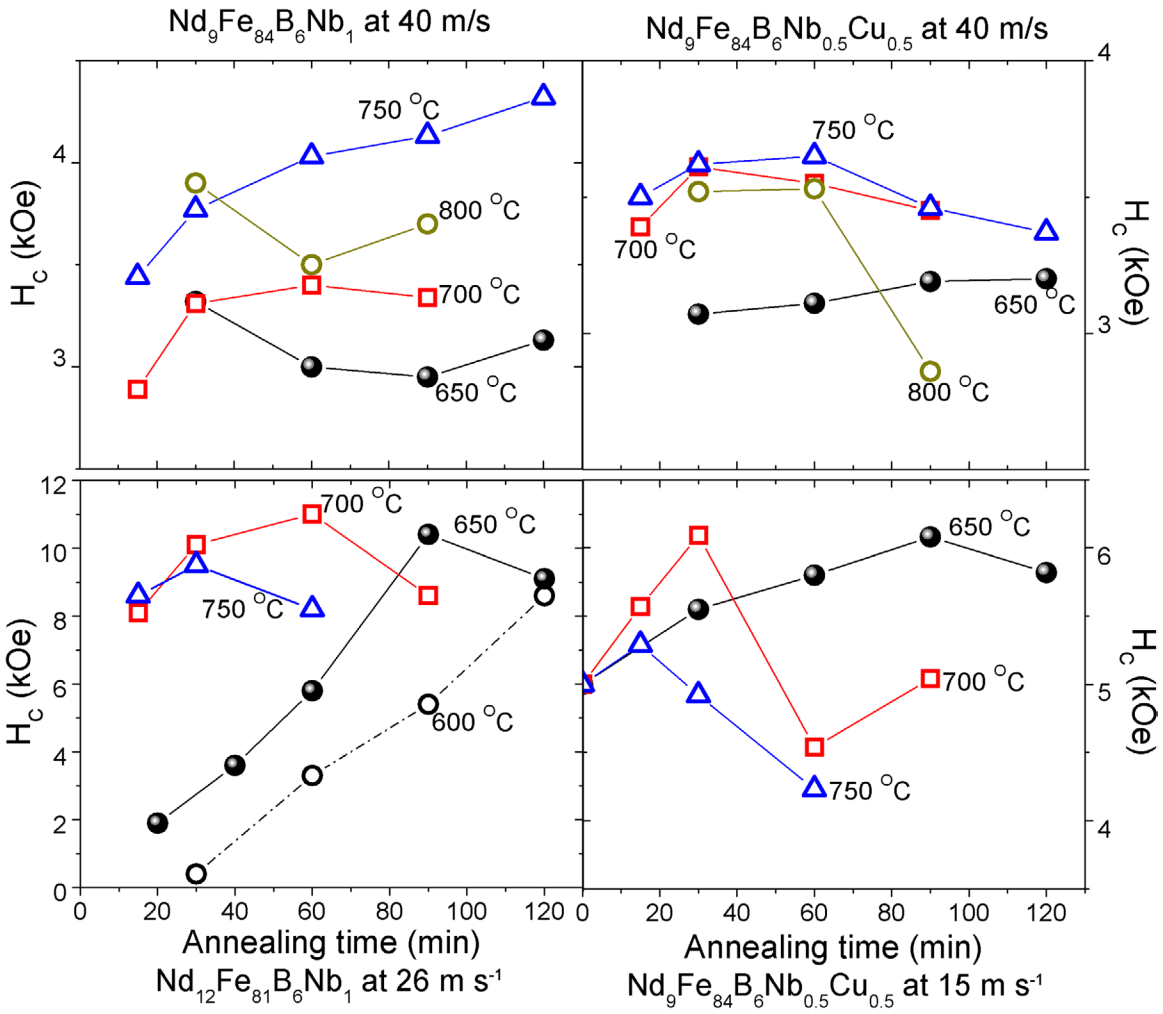

Figure 5. Coercive field of ribbons heat-treated at different temperatures and times.

and decreases on samples heat-treated at 750 °C for more than 90 min. This value is higher than the one obtained in 9NFBN_40 at the same annealing temperature (H_c ~ 3.3 kOe). This effect was not observed in the 9NFBN_40 ribbon samples, where H_c increases progressively with annealing at 750 °C up to 120 min. In both cases, the use of higher annealing

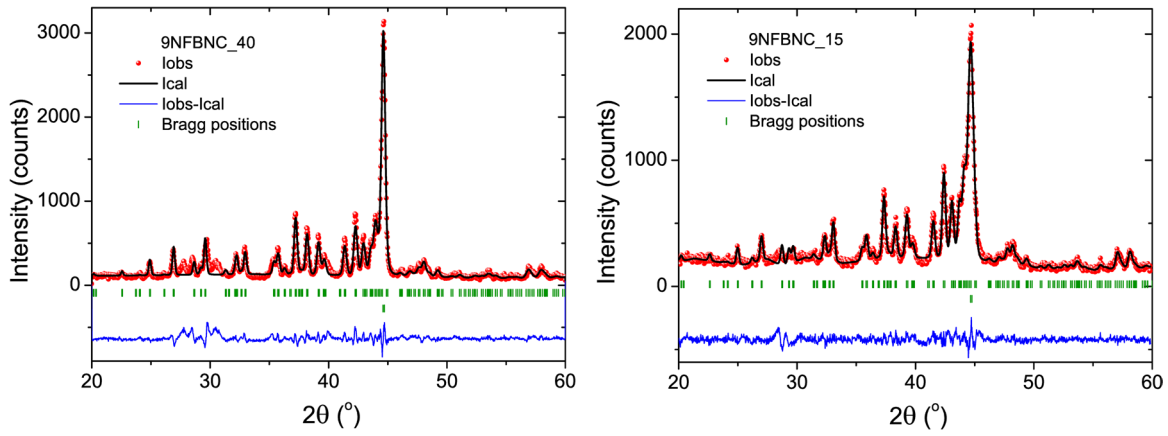

Figure 6. Refinement of XRD profiles of (a) 9NFBNC_40 and (b) 9NFBNC_15 with maximum H_c by means of the Rietveld method.

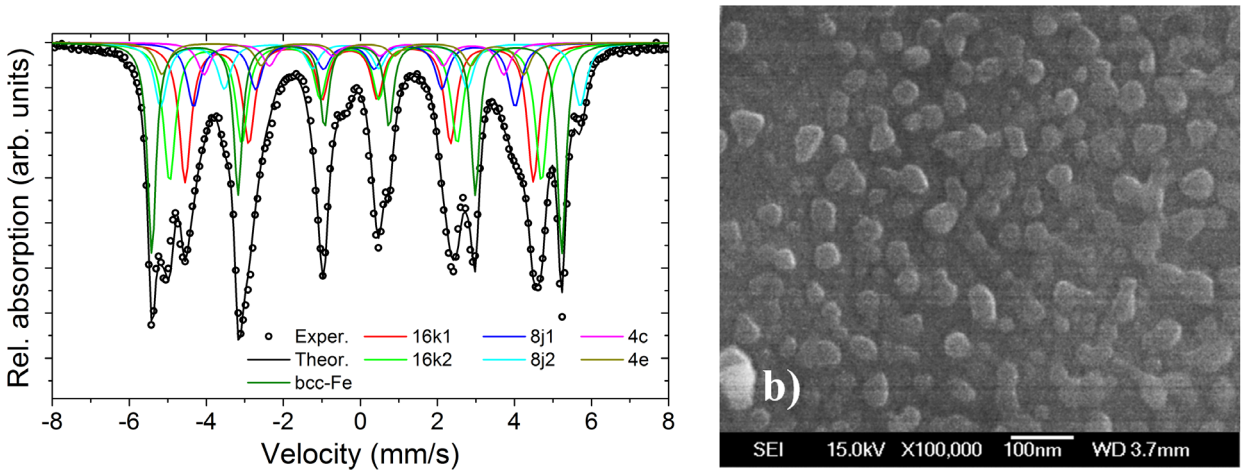

Figure 7. (a) Mössbauer spectra (at room temperature) of sample 9NFBNC_40 heat-treated at 750 °C for 60 min and (b) SEM image of 12NFBN_26 heat-treated at 700 °C for 60 min.

temperatures (800 °C) is detrimental to the desired magnetic hysteresis behavior due to the excessive growth of α-Fe phase at these temperatures.

It is clear that these results have not yet produced the best magnetic hysteresis behavior expected in this system, possibly due to the difficulty in obtaining larger grain sizes while, at the same time, avoiding the formation of a large α-Fe phase. In order to obtain a grain size closer to the optimum, with the right amount of soft magnetic phase, a nanocrystalline ribbon of 9NFBNC_15 was prepared by spinning at 15 m s^{-1}, which led to a nanocomposite structure in the as-spun ribbons with a relatively high H_c (>5 kOe), due to the proper grain size and lack of excess α-Fe phase. The highest coercivity ($H_c > 6$ kOe) is obtained at a considerably lower annealing temperature (650°C–90 min) or higher temperature, but for a shorter time (700 °C–30 min) than those obtained in the amorphous ribbons.

3.4. Nanostructure of the optimal samples

XRD was carried out on ribbons with the highest H_c values and analyzed by the Rietveld method to evaluate the ratio of the different phases present. Results for the heat-treated 9NFBNC_40 and 9NFBNC_15 samples are shown in figure 6. XRD spectra for all samples are summarized in the supplementary material file. Two phases, defined as $Nd_2Fe_{14}B$ and α-Fe, are present. The lattice parameters of the $Nd_2Fe_{14}B$ phase are $a = 8.80 \pm 0.02$ Å, $c = 12.21 \pm 0.02$ Å and do not change with the heat treatments. The amount of each phase obtained by this procedure is rather unreliable, as it seems to be a pronounced texture in most samples. For example in 10NFB_26 heat-treated sample, the amount of α-Fe phase was estimated as 60%, much higher than the nominal value (16.7%), whilst for 12NFBN_26 this value (5%) was close to its nominal (0%). For this reason, we used Mössbauer spectroscopy to obtain the amounts of different Fe-rich phases in the heat-treated samples.

$Nd_2Fe_{14}B$ alloys have been studied extensively in the past by Mössbauer spectroscopy [18, 19]. This phase presents six non-equivalent crystallographic sites for Fe, 16k_1, 16k_2, 8j_1, 8j_2, 4e, and 4c sites. The assignment of the six magnetic sextets to the six crystallographic iron sites is the usual one [18, 19]. In order to independently determine the distribution of the Fe atoms after crystallization among the bcc-Fe and $Nd_2Fe_{14}B$ phases, the relative areas of the six sextets were constrained to the site populations, i.e. 16:16:8:8:4:4.

The Mössbauer spectra observed in figure 7(a) for 9NFBNC_40, were fitted using six Fe-sites corresponding to the 2:14:1 phase and one Fe-site for bcc-Fe. At room

Table 2. Summary of best heat-treated samples, heat treatments, coercive field, saturation magnetization, normalized remanence, phase contents obtained by Mössbauer and estimated from nominal composition (in brackets) and grain size of 2:14:1 hard phase observed with XRD and SEM, when available (in brackets).

Sample	HT (°C min)	H_c (kOe)	M_s (emu g^{-1})	M_r/M_s	$Nd_2Fe_{14}B$ (%)	α-Fe (%)	Grain size (nm)
10NFB_26	650–60	5.1	123	0.71	84.7(83.3)	15.3(16.7)	80(125)
9NFBNC_40	750–60	3.7	169	0.57	75.2(75)	23.8(25)	>100
9NFBN_40	750–120	4.3	143	0.64	82.7(75)	17.3(25)	88
9NFBNC_15	700–30	6.1	148	0.64	78.2(75)	21.8(25)	>100(90)
12NFBN_26	700–60	11	106	0.72	94.2(100)	5.8(0)	98(48)

temperature, these phases show ferromagnetic ordering, as is evidenced by their corresponding sextets in the spectra. The results of the Mössbauer spectra analysis are summarized in table 2. As can be seen, the amount of each phase is close to the nominal one, which is estimated from the Fe excess in the initial alloy composition (displayed in table 2).

The sample with highest coercivity (11 kOe) is the stoichiometric one: 12NFBN_26. This sample shows the lowest value of the α-Fe phase (5.8%) and saturation magnetization (106.5 emu g^{-1}) and has the best coupling between the hard and soft phases, as deduced from the highest m_R value of 0.72. The sample 9NFBNC_40, heat-treated at 750 °C for 60 min, shows the lowest coercivity (3.7 kOe). This sample has the highest amount of α-Fe phase (23.8%) and largest value of saturation magnetization (169.3 emu g^{-1}). Large amounts of α-Fe usually worsen the exchange coupling, as reflected by the corresponding value of $m_R = 0.57$, which is the lowest one in the series. However, the same sample 9NFBNC_15 spun at a lower wheel speed, shows a crystalline order (see figure 1(a)). It has the largest coercivity (6.1 kOe) (one of the highest values reported in Nd-lean samples) in the as-quenched state and a slightly higher $m_R = 0.64$, which indicates a better exchange coupling in this sample. However, its high α-Fe content still runs counter to a stronger exchange coupling.

In order to analyze the dependence of the hard magnetic properties on the microstructure of the samples, we measured the grain size by SEM. An SEM micrograph of the heat-treated 12NFBN_26 sample is shown in figure 7(b). The values of grain size for each sample are summarized in table 2, together with those calculated by XRD. The latter are not reliable, because values close to 100 nm lie in the upper limit for a correct size estimation by x-ray. The data show that the optimum grain size for maximum coercivity, which is at the single/multi-domain threshold (~75–120 nm) [20], was reached in most samples. Recent predictions made on nanocomposite Nd–Fe–B/α-Fe magnets by micromagnetic simulations suggest that the effect of the volume fraction or the magnetocrystalline anisotropy of the bcc-Fe phase on exchange coupling, generally exceed the influence of the grain size [21].

The values of coercivity in exchange-coupled Nd-lean samples are lower than in over-stoichiometric samples. It would be very interesting to study the effect of infiltration of a eutectic rare-earth-rich alloy at the grain boundaries to try to increase the coercivity in order to make these Nd-lean materials suitable for permanent magnets.

4. Conclusions

A study of the crystallization process was performed on Nd-lean Nd–Fe–B melt-spun alloys with Nb and Cu doping. The microstructure of as-spun ribbons can be controlled by varying the wheel speed, allowing the reduction of the annealing temperature in nanocrystalline samples (those spun at a lower wheel speed) and the preparation of highly disordered ribbons in the case of high wheel speed. The crystallization processes in these materials show (in all cases) the formation of two magnetic phases: the 2:14:1 hard magnetic phase at temperatures between 280–400 °C and a secondary α-Fe soft magnetic phase around 600 °C. The grain growth during the heat treatments can be controlled by the addition of Nb and Cu, showing inhibition of growth by Nb and a nucleation at lower temperatures in samples with Cu. However, the early formation of 2:14:1 phase by heat treatment helps the crystallization of the secondary α-Fe phase. We can conclude that the formation of the latter phase is also driven by doping and, furthermore, is detrimental to the exchange coupling in our nanostructured magnets.

Acknowledgments

This work has received funding from the DOE BES-DE-FG02-90ER45413 and the European Union MSCA grant agreement No 691235 (INAPEM). Technical and human support provided by SGIker (UPV/EHU, GV/EJ and ESF) is gratefully acknowledged.

References

[1] Anon 2011 Tackling the challenges in commodity markets and on raw materials *COM 25*
[2] Madugundo R, Salazar-Jaramillo D, Manuel Barandiaran J and Hadjipanayis G C 2016 High coercivity in rare-earth lean nanocomposite magnets by grain boundary infiltration *J. Magn. Magn. Mater.* **400** 300–3
[3] Gabay A M and Hadjipanayis G C 2016 ThMn12-type structure and uniaxial magnetic anisotropy in $ZrFe_{10}Si_2$ and $Zr_{1-x}Ce_xFe_{10}Si_2$ alloys *J. Alloys Compd.* **657** 133–7
[4] Withanawasam L, Murphy A S, Hadjipanayis G C and Krause R F 1994 Nanocomposite $R_2Fe_{14}B$/Fe exchange coupled magnets *J. Appl. Phys.* **76** 7065
[5] Zeng H, Li J, Liu J P, Wang Z L and Sun S 2002 Exchange-coupled nanocomposite magnets by nanoparticle self-assembly *Nature* **420** 395–8

[6] Yue M, Li Y, Wu Q and Liu W 2014 Bulk nanostructural permanent magnetic materials *Rev. Nanosci. Nanotechnol.* **3** 276–88
[7] Sen Y, Shandong L, Xiansong L, Xiaoping S, Benxi G and Youwei D 2002 Exchange coupled Nd2Fe14B/α-Fe nanocomposite magnets with fine α-Fe grains obtained by low wheel speed spinning *J. Alloys Compd.* **343** 217–22
[8] Men K, Li K, Luo Y, Yu D, Zhang K, Jin J and Mao Y 2015 The crystallization behavior of as-quenched $Nd_9Fe_{85}Nb_{0.5}B_{5.5}$ alloys *J. Alloys Compd.* **635** 61–5
[9] Zhou W, Chang C, Inoue A, Wang X, Li F and Huo J 2015 Direct production of hard magnetic ribbons with enhanced magnetic properties by controlling cooling rate of melt *J. Appl. Phys.* **117** 123905
[10] David S and Givord D 1998 Coercivity in lean rare earth NdFeB and PrFeB nanocomposite hard magnetic materials *J. Alloys Compd.* **281** 6–11
[11] Li W, Li L, Nan Y, Li X, Zhang X, Gunderov D V, Stolyarov V V and Popov A G 2007 Controllable nanocrystallization in amorphous $Nd_9Fe_{85}B_6$ via combined application of severe plastic deformation and thermal annealing *Appl. Phys. Lett.* **91** 62509
[12] Zhang S Y, Xu H, Ni J S, Wang H L, Hou X L and Dong Y D 2007 Microstructure refinement and magnetic property enhancement for nanocomposite $Nd_2Fe_{14}B$/α-Fe alloys by Co and Zr additions *Physica* B **393** 153–7
[13] Chiriac H, Marinescu M, Buschow K H, de Boer F and Brück E 1999 Influence of the annealing procedures on magnetic properties of α-Fe/$Nd_2Fe_{14}B$ nanocrystalline alloys *J. Magn. Magn. Mater.* **202** 22–6
[14] Zhang R, Liu Y, Ye J, Yang W, Ma Y and Gao S 2007 Effect of Nb substitution on the temperature characteristics and microstructures of rapid-quenched NdFeB alloy *J. Alloys Compd.* **427** 78–81
[15] Wu Y Q, Ping D H, Hono K, Hamano M and Inoue A 2000 Microstructural characterization of an α-Fe/$Nd_2Fe_{14}B$ nanocomposite magnet with a remaining amorphous phase *J. Appl. Phys.* **87** 8658
[16] Morrish A H 2001 *The Physical Principles of Magnetism* (New York: Wiley-VCH)
[17] Kneller E F and Hawig R 1991 The exchange-spring magnet: a new material principle for permanent magnets *IEEE Trans. Magn.* **27** 3588–60
[18] Grandjean F, Long G J, Pringle O A and Fu J 1990 A Mössbauer effect study of the $Re_2Fe_{14}B$ magnets, where RE is Y, Pr, Nd, and Gd *Hyperfine Interact.* **62** 131–46
[19] Long G J, Kulasekere R, Pringle O A, Grandjean F and Buschow K H J 1992 A comparison of the Mössbauer effect spectra of $R_2Fe_{14}B$ and $R_2Fe_{14}C$ *J. Magn. Magn. Mater.* **117** 239–50
[20] Girt E, Krishnan K M, Thomas G, Girt E and Altounian Z 2001 Coercivity limits and mechanism in nanocomposite Nd–Fe–B alloys *J. Magn. Magn. Mater.* **231** 219–30
[21] Sepehri-Amin H, Dirba I, Schwöbel C, Ohkubo T, Hono K and Gutfleisch O 2016 Design of nanocomposite Nd–Fe–B/Fe magnets using micromagnetic simulation *The 24th Int. Workshop on Rare-Earth and Future Permanent Magnets and Their Applications (REPM2016)* p 101